Supplemental Figures and Legends

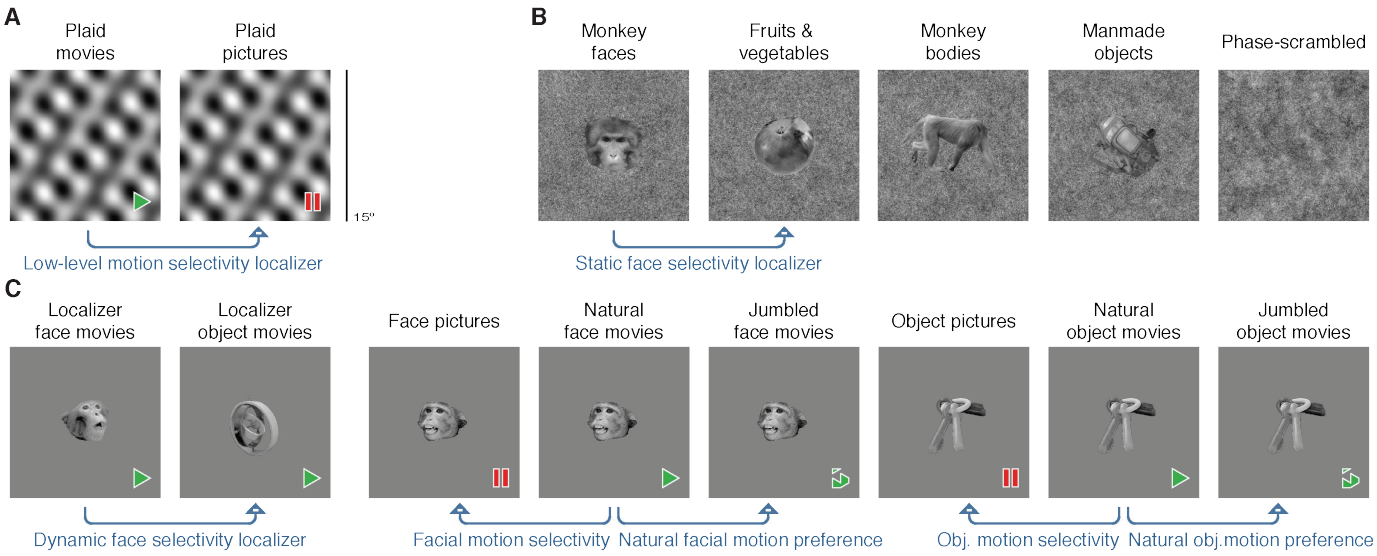

Figure S1. Example Stimuli, Related to Experimental Methods

(**A**) Sample frames from the low-level motion stimulus set and definition of contrast (blue arrow) for measuring low-level motion selectivity. (**B**) Sample stimuli from the object category stimulus set and definition of the static face selectivity contrast. (**C**) Sample frames from the object motion stimulus set and definition of related contrasts. Note that the source movies used to create the stimuli for the dynamic face selectivity contrast were different than the source movies used for the other blocks of this stimulus set; they featured the same monkeys and cage toys demonstrating different actions. We used data collected in response to the localizer movies *solely* to localize the face patch ROIs, and based all analyses within these ROIs on independent data collected during the presentation of other stimuli.

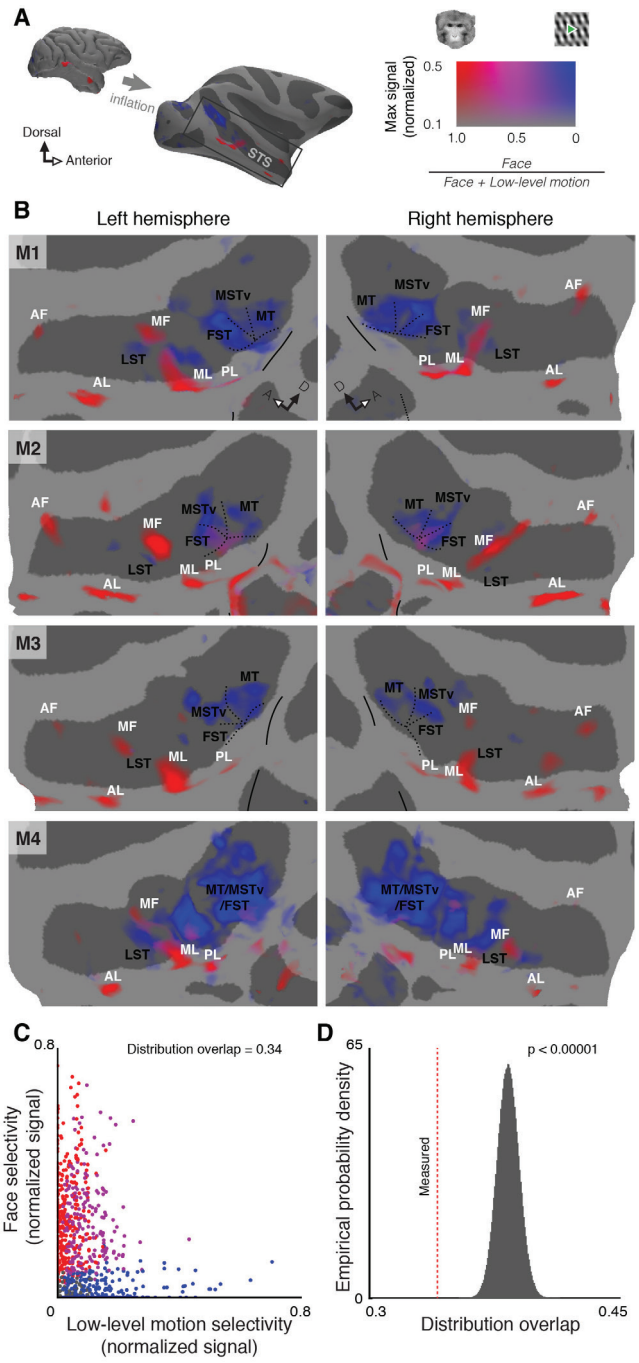

Figure S2. Spatially Dissociated Selectivities for Static Faces and Low-Level Motion in the STS Fundus, Related to Figure 1

(**A**) Left: face form selectivity (red; faces - fruits & vegetables) and low-level motion selectivity (blue; plaid movies - plaid pictures) plotted on an inflated model of M1's right cortical hemisphere. The gray box highlights the region depicted below in B. Right: the hue at each point reflects the relative strength (normalized signal change) of these two contrasts, and opacity reflects the strength of the strongest contrast. (**B**) Flattened maps, as in panel A, of the STS of each hemisphere in 4 subjects. Face patches (white text) and motion areas (black text) are labeled according to the criteria described in Experimental Methods. Dotted lines represent retinotopic meridians used to identify motion areas and solid lines represent retinotopic meridians at the anterior edge of area V4. Note how there is widespread separation of face selectivity and low-level motion selectivity. We found just one exception to this rule of spatial segregation of function: in M2 and M4 the ventral, foveal aspect of the MT/MSTv/FST motion complex exhibited face selectivity (similar to area pPL of [S1]) (**C**) Scatter plot of joint face and motion selectivity of voxels in the fundus of the STS (as defined by sulcal depth). Static face selectivity and low-level motion selectivity (signal change, normalized per subject) were determined for voxels in the fundus of the STS (excluding the MT/MSTv/FST complex, see Supplemental Experimental Methods) most responsive to movies of faces or objects. Dot color represents significant ($q < 0.01$) stimulus selectivities of each voxel: red for static face selectivity (faces - fruits and vegetables), blue for low-level motion selectivity (plaid movies - plaid pictures), magenta for both. These selectivity distributions

had a voxel-wise distribution overlap value (DOV) of 0.34 (see Supplemental Experimental Methods). (**D**) Determination of statistical significance of measured DOV. The gray plot shows the null distribution of DOV, under the assumption of a random association between static face-selectivity and low-level motion selectivity across the considered voxels. The dashed red line represents the measured DOV of 0.34 (from panel A). This value is very significantly ($p < 0.00001$) smaller than expected by chance associations. Thus face and motion selectivity are neither co-localized nor independently distributed in the fundus of the STS, but are spatially segregated. Alternative quantifications of similarity of these stimulus selectivity distributions using cosine distance and Spearman correlation confirmed that they were less similar than would be expected by chance (both $p < 0.0005$). These *p*-values reflect upper (less significant) limits of 99% confidence intervals (see Supplemental Experimental Methods).

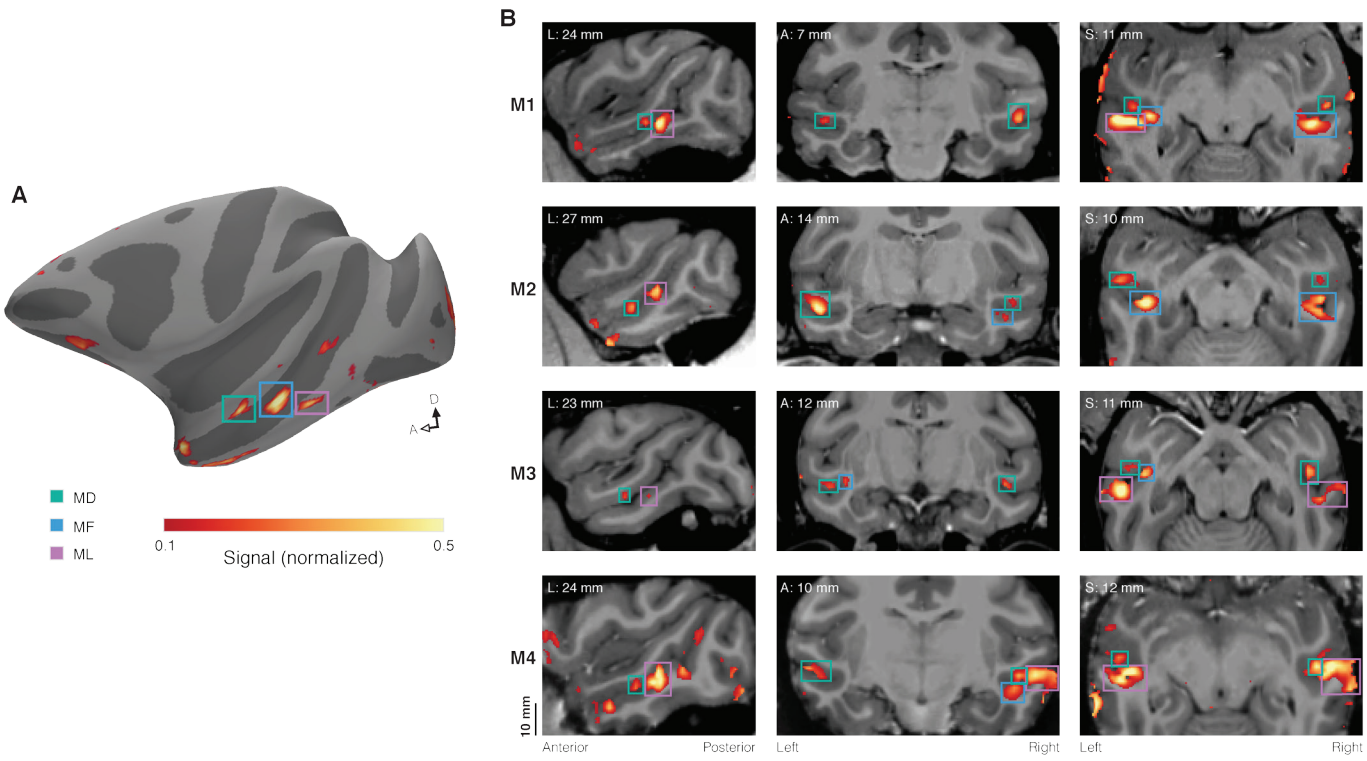

Figure S3. Identification and Location of the Middle Dorsal Face Patch (MD), Related to Figure 2

(**A**) Inflated cortical surface model of M2's left hemisphere showing the relative locations of ML (purple), MF (blue), and MD (green). (**B**) Slice representations of the middle face patches (ML, MF, and MD) in all subjects (top to bottom). Parasagittal slices (left column) show the left hemispheres. Coronal and horizontal slices (center and right column, respectively) are presented following neurological convention, with the right side of the brain on the right side of the page. Slice coordinates assume standard stereotaxic positioning and are measured from the midpoint of the interaural line. The coronal slice of M2 is the one shown in Figure 2B and is reproduced here for completeness. Functional maps show the dynamic face selectivity localizer thresholded at an FDR of $q < 0.01$.

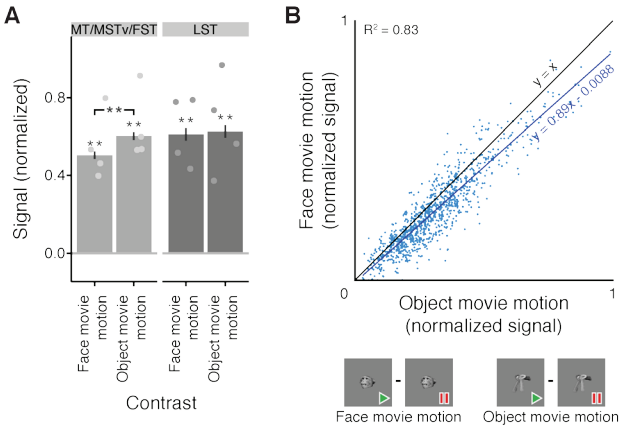

Figure S4. Analysis of Motion Content in Face and Object Movies, Related to Figure 2

(**A**) Responses of two ROIs, MT/MSTv/FST complex and LST, to two stimulus contrasts, face movie motion (natural face movies - face pictures; "face motion selectivity" in Figure S1C) and object movie motion (natural object movies - object pictures; "object motion selectivity" in Figure S1C). Both motion selective regions responded just as much (LST) if not more (MT/MSTv/FST) to the motion in the object movies than to the motion in the face movies. * = $p < 0.05$ and ** = $p < 0.01$, corrected using Holm–Bonferroni method for 6 tests (2 ROIs × (2 measures + comparison)). Dots on bar plots represent the values for individual subjects. Signal change is normalized per ROI. Error bars represent standard error. The data from LST are the same as those presented in Figure 2E-G. (**B**) Response of the 250 voxels in each subject's temporal lobe most responsive to low-level motion (as measured by the low-level motion selectivity localizer) to face movie and object movie motion. Responses to the two types of motion are highly correlated. Linear regression suggests that the voxels in the temporal lobes most sensitive to low level motion responded ~89% as strongly to motion in the face movies as they responded to motion in the object movies. Signal change is normalized per subject. Both analyses suggest that motion content in face and object movies was well matched, and if not entirely equal, slightly larger in object movies than in face movies.

Supplemental Experimental Procedures

All procedures conformed to local and NIH guidelines, including the NIH Guide for Care and Use of Laboratory Animals. These experiments were performed with the approval of the Institutional Animal Care and Use Committees of The Rockefeller University and Weill Cornell Medical College.

Subjects

We studied four male rhesus monkeys (*Macaca mulatta*), aged 3.5 to 5 years old, weighing 5.5 to 7.5 kg. A cranial implant composed of acrylic cements (C&B-Metabond, Parkell; Palacos LV+G, Zimmer) and anchored with ceramic screws (Thomas Recording; Rogue Research) was implanted in each monkey using standard surgical methods, and standard anesthetic and postoperative treatment protocols were followed. A custom-designed MRI-compatible headpost made of Ultem (SABIC) was secured in each implant.

Data Acquisition

We acquired all MRI data with a 3T Siemens Tim Trio MRI scanner, using an AC-88 gradient insert (Siemens) for functional scans. Immediately prior to each functional scan, a dose of Feraheme (AMAG Pharmaceuticals; M1-M3) or Molday ION (BioPAL; M4) containing 8 to 10 mg/kg of iron was injected into a saphenous vein to increase functional contrast. When Molday ION was administered on consecutive days, we adjusted the dosage to compensate for functional half-life. As these agents increase functional contrast by decreasing local MR signal [S2, S3], we inverted the sign of our measurements during analysis so that positive values reflect increased blood volume. Functional images were obtained with a custom-designed 8-channel surface coil (Lawrence Wald, MGH Martinos Center) and a gradient-echo echo-planar imaging sequence with 54 horizontal slices, a 96 ×

96 in-plane matrix, an isotropic resolution of 1 mm^3, TR = 2 s, TE = 16 ms, and 2 × GRAPPA acceleration.

We acquired 6 anatomical MRI volumes from each subject to serve as the basis for individualized models of the cortical surface. With the subject under isoflurane anesthesia and positioned in an MRI-compatible stereotactic frame, T1-weighted images were obtained using a custom single-channel surface coil and a fast gradient echo sequence (magnetization-prepared rapid gradient echo, MPRAGE) with 240 sagittal slices, an in-plane matrix of 256 × 256, and an isotropic resolution of 0.5 mm^3.

Visual Stimuli

During functional scans, stimuli were projected at 60 Hz onto a screen placed 35 cm in front of the monkey's eyes. Three block design stimulus sets were presented to each subject: low-level motion, object category, and object motion (Figure S1). A fourth stimulus set for retinotopic mapping was presented to M1 to M3.

The low-level motion stimulus set (Figure S1A) consisted of two types of stimuli: dynamic and static. Dynamic blocks contained movies of shifting plaids created by superimposing two drifting sinusoidal gratings [S4]. The gratings drifted linearly with a period of 1/3 s and were randomly reoriented after a single period (3 times per second). The static blocks consisted of still frames taken from these movies. The frames of the static stimuli were updated every 1/6 s (every half period) so that 2 frames were shown for each plaid: an initial image and its negative. Thus, while there was a strong percept of translational movement throughout the dynamic blocks, this was removed in the static blocks. These stimuli were presented in the scanner at 15° × 15° and 30 fps. A single run of this stimulus set consisted of 36 s of gray, 6 stimulus blocks of 24 s alternating between dynamic and static, 24 s of gray, the 6 stimulus blocks shown in reverse order, and a final 24 s of gray. 2 different

orders were used: one where a static block came first and one where a dynamic block came first. 16, 10, 8 and 16 runs of this stimulus set were analyzed, respectively, for M1 to M4.

In the object category stimulus set (Figure S1B), grayscale pictures of rhesus macaque faces, cynomolgus macaque faces, fruits and vegetables, monkey bodies, and manmade objects were presented in separate 24 s blocks. An additional block, composed of phase-scrambled versions of the fruit and vegetable pictures, was also presented. In this study, we used this stimulus set to localize the face patches by comparing the responses to monkey faces with the responses to fruits and vegetables; both blocks of monkey faces were combined for this analysis. Each block of this stimulus set consisted of 15 exemplar images shown for 0.4 s, with each exemplar repeated 4 times in a block. Images were matched within and across all categories for total screen area, placed on a pink noise background, and normalized for luminance and frequency amplitude (http://www.mapageweb.umontreal.ca/gosselif/shine [S5]). In addition, images were chosen so that the aspect ratios of the fruits and vegetables matched those of the macaque faces, and the aspect ratios of the manmade objects matched those of the macaque bodies. At the scanner, the pink noise background was presented at 15° × 15°, and the average foreground image was 7.1° × 5.5°. Each image was presented at 1 of 5 equally likely screen positions: either at the center or offset 1.1° from the center to the left, right, top, or bottom. A Latin square design was used to create 6 orders of the stimulus blocks, so that both the relative position of each block within a run and the identity of the immediately preceding block were balanced. Each run of this stimulus set consisted of 36 s of gray, followed by the 6 stimulus blocks without intervening gaps, 24 s of gray, the 6 blocks presented in reverse order, and a final 24 s of gray. In cases where matched sets of all 6 orders were not available for analysis, the palindromic design of the runs allowed balance to be achieved by analyzing matched sets of 3 orders. 36, 30, 27, and 30 runs of this stimulus set were analyzed, respectively, for M1 to M4.

The object motion stimulus set (Figure S1C) consisted of stimuli showing either familiar macaque faces ('faces') or familiar cage toys ('objects') as 'pictures', 'natural movies', or 'jumbled movies'. Picture, natural movie, and jumbled movie stimuli were created from a common set of videos: picture blocks showed the videos at 2 fps, natural movie blocks showed them at 15 fps, and jumbled movie blocks showed the same frames in randomized order at 15 fps (Figure 3A). Independent videos were used to create an additional block of natural face movies and an additional block of natural object movies to use for the localization of face patches (in Figure 2A); we refer to these as 'localizer movies'. Each block of this stimulus set consisted of 6 exemplar movies/image sequences shown for 3 s apiece. Source videos of both monkeys and objects were recorded at 60 fps to minimize motion blur. The cage toys shown in the object blocks were all able to undergo non-rigid movement to better match the range of transformations demonstrated by the monkey faces, and object videos showing vigorous movement were captured to ensure that motion content was no greater in the face videos than in object videos (also, see Figure S4). Stimulus subjects were recorded in front of a blue screen under a standardized set of lighting conditions, monkey bodies were masked with a blue neck plate, and chroma keying was carried out in Final Cut Pro (Apple) so that the subjects could be isolated from the background and videos could be standardized. An exemplar frame from each video was used to standardize the pixel area of the subjects to an equivalent circular diameter, the centers of all subjects' trajectories were aligned, color was removed, and luminance was histogram-normalized across all frames [S5]. At the scanner, the resulting stimuli were shown with the subjects having an equivalent circular diameter 8.5º and moving within a 15º x 15º middle gray background. Again, a Latin squares design was used, resulting in 8 counterbalanced orders. Each experimental run was composed of 24 s of gray, the 8 stimulus blocks (18 s apiece), 24 s of gray, the stimulus blocks in reverse order, and a final 30 s of gray. Palindromic design again allowed for balance with matched sets of 4 orders when available runs were not balanced across all 8 orders. 48, 32, 20 and 40 runs of this stimulus set were analyzed, respectively, for M1 to M4.

The retinotopic mapping stimulus that we showed to M1-M3 consisted of a bar containing a high contrast moving pattern (the shifting plaids of the low-level motion stimulus) crossing a gray visual field in 8 directions [S6]. The circular area traversed by the bar was 30º in diameter at the scanner. This stimulus began with a 30 s period of gray, each crossing of the bar took 32s, and 20s periods of gray were placed after every 2 crossings. 19, 31, and 17 runs of this stimulus set were analyzed for M1, M2, and M3, respectively.

Data Analysis

We carried out the preprocessing of our fMRI data in a way designed to account for the artifacts most common to imaging of head-fixed, awake monkeys (see discussion in [S7]). To correct for image changes resulting from head and body motion, slice-wise correction within each run was carried out using AFNI's 3dAllineate (http://afni.nimh.nih.gov) and included terms for cubic warping in the phase-encoding direction, as well as shifts, rotations, scaling, and skewing within each slice. We then slice-time corrected all runs with FreeSurfer's functional analysis stream, FS-FAST [S8], and used mutual information-based non-linear alignment (JIP, http://www.nitrc.org/projects/jip [S9]) to compensate for static distortions of the functional volumes in each experiment and align these volumes to the high-resolution anatomical scans that we used for cortical surface modeling.

We analyzed the preprocessed data resulting from the low-level motion, object category and object motion stimuli with FS-FAST, as described previously [S8, S10]. For retinotopic mapping, we fit a PRF (population receptive field) model to the recorded data using mrVista (http://vistalab.stanford.edu/software/ [S6]); as in the FS-FAST analysis, a wide hemodynamic response function was used in modeling to match the expected effect of the contrast agent [S2, S3].

When mapping functional data, either within brain volumes or on cortical surface models, we considered two outputs of our fMRI analysis: the percent signal change of a voxel (either between baseline and a stimulus block or between linear combinations of stimulus blocks) and the statistical

significance of this percent signal change. Because of inter-subject differences, including MRI coil placement and contrast agent clearance, a given percent signal change does not reflect the same degree of hemodynamic activity in every subject. To compensate for this, signal change was normalized by separately scaling each subject, dividing signal change values of every voxel by the maximal signal change seen in the STS for a contrast of interest. Signals from the low-level motion experiment were normalized by finding the voxel in the STS with the highest percent signal difference between plaid movies and plaid pictures and dividing all percent signal change values from the same animal by that number. The object category experiment was normalized by the maximum value of the static face-selectivity localizer within the STS and the object motion experiment was normalized by the maximum STS value of the dynamic face-selectivity localizer. Because these normalizations were constant multiplicative scaling within each subject, they had no effect on the statistical significance of the maps. Significance values for the maps were adjusted for multiple comparisons by considering all voxels (cortical, subcortical, and cerebellar) within a whole brain mask and using the Benjamini-Hochberg procedure to calculate *q* values representing false discovery rate [S11].

A model of each monkey's cortical surface was created from the anesthetized anatomical scans using FreeSurfer (http://surfer.nmr.mgh.harvard.edu [S8, S10]). Data (signal changes and *q* values) were projected from voxels in the midway point of the cortical sheet onto cortical surface models using trilinear interpolation. Images of cortical surface models with functional overlays were rendered using custom code in MATLAB (The MathWorks), while images of volume slices with functional overlays and the volumetric reconstruction of ROIs (Figure 2C) were created in Slicer (http://www.slicer.org).

We analyzed the spatial similarity of the anatomical distributions of static face selectivity and low-level motion selectivity in the fundus of the STS (Figure S2C-D) by using the overlapping coefficient (hereafter referred to as 'distribution overlap'). We restricted our analysis to parts of the STS with a concave curvature and anterior to the MT/MSTv/FST complex, as parts in this complex or

along the lips of the STS generally show clear separation of face and low-level motion signals [S12]. To identify voxels in the STS fundus that would be likely driven by our stimuli, we subselected from these voxels, choosing the 500 in each subject with the greatest significant signal change in response to either the localizer face movie or the localizer object movie (Figure S1C); note that these data were not used to calculate either of the functional maps being compared. We then looked, per voxel, at the selectivity for static faces and low-level motion (normalized per subject) and measured their similarity across the 2000 voxels. Distribution overlap was calculated by normalizing the sum of each contrast over all 2000 voxels to 1, and then summing the lesser of these two normalized distributions on each voxel over all voxels. To determine the significance of this overlap, we used a Monte Carlo permutation test. We created an empirical null distribution (Figure S2D) by randomizing the pairing of the two compared contrasts across the considered voxels within each monkey 1,000,000 times and recording the resulting distribution overlap each time. We calculated the 99% confidence interval of the resulting *p* value according to the binomial distribution (see [S13]). We report the upper (less statistically significant) bound of this confidence interval.

ROIs were defined in each hemisphere of each animal and combined into bilateral ROIs for analysis. Within a hemisphere, we positioned each ROI by finding a voxel showing a local maximum signal change in an area, selecting a 3 x 3 x 3 voxel region centered on this point, and excluding all voxels that did not meet a $q < 0.05$ significance criterion. If multiple maxima were found which could represent a given area of interest, we chose the one that maximized the symmetry between the hemispheres of a subject.

ROIs were named based on both anatomical and functional characteristics. Face patches were identified using the dynamic face localizer and named based on anatomical location and relative position [S14]. The toy patch was also identified using the dynamic face localizer, and was defined by responding more to object movies than face movies. Because there were a number of such areas in each hemisphere (and no existing classification scheme), we chose the most anterior local maximum

that was posterior to AL in each hemisphere, as we found that this region reliably neighbored both face patches and areas responding to low-level motion (generally, LST). LST was identified as a motion-sensitive area (as identified by the pattern motion localizer) in the lower bank of the STS and anterior to area FST [S15]. MT/MSTv/FST (analyzed in Figure S4) was identified as a motion-sensitive area (as identified by the pattern motion localizer) with appropriate retinotopic organization (M1-M3) and anatomical location [S16]. Because the MT/MSTv/FST complex is a functionally heterogeneous region with known retinotopic organization, it was important to define an ROI that spanned this functional diversity and was not overly influenced by a single area or retinotopic preference. The ROI identification scheme used in other regions (a 3 × 3 voxel ROI centered on a local signal maximum) created ROIs that were too spatially limited to meet these criteria. Therefore, we took another approach to define this ROI. We used the low-level motion selectivity localizer (Figure S1A), set a significance threshold with $q \ll 0.01$ and q small enough that there was no contiguous path of voxels meeting the threshold between the retinotopic center of MT/MSTv/FST and other motion-selective regions. All contiguously connected voxels meeting this threshold were considered part of the MT/MSTv/FST ROI (as in [S12]).

For group analysis, we independently normalized the time courses from each ROI of each monkey and subjected them to a fixed effects analysis, pooling runs across all monkeys. We did this in two steps. In the first step, the time courses of all voxels within a given monkey and ROI were averaged and the resulting ROI time courses were analyzed with FS-FAST, just as if each ROI was a standard functional voxel. This allowed us to calculate responses within each ROI that could be used for normalization in the second step. In the second step, we normalized the time courses for each ROI in each monkey independently before performing a fixed effects analysis across all monkeys. Note that this is different than the pan-brain per-subject normalization that we performed for the mapping analyses; we chose this alternate approach because differences in signal distribution (see [S17]) and hemodynamic effects [S18] can occur across the brain – not only between subjects – and

it is important to minimize these differences as much as possible prior to a fixed effects analysis. For the object category experiment, time courses in each face patch were divided by the response to the rhesus faces in that patch. For the object motion experiment, time courses in each face patch were divided by the response to the localizer face movies in that patch, while time courses in LST and the object patch were normalized by the response to the localizer object movies in that ROI. Because each ROI was independently normalized, comparisons between ROIs should be drawn with care, keeping in mind that each signal change is dependent on the response to the condition used for normalization. These normalized ROI time courses were then analyzed across all 4 monkeys using a fixed effects analysis in FS-FAST. We used a fixed effects analysis (as is common in monkey fMRI experiments [S12, S19]) because our sample size was too small for effective power in a random effects analysis [S20] despite our comparatively large number of subjects (see [S1, S12, S21]). Statistical conclusions drawn from fixed effects analyses generalize only to the sample under study (see discussion in [S22]). We adjusted the *p* values of ROI analyses for multiple testing using the Holm-Bonferroni method to control for familywise error rate [S23].

Supplemental References

S1. Janssens, T., Zhu, Q., Popivanov, I. D., and Vanduffel, W. (2014). Probabilistic and single-subject retinotopic maps reveal the topographic organization of face patches in the macaque cortex. J. Neurosci. *34*, 10156–10167.

S2. Mandeville, J. B., Marota, J. J., Kosofsky, B. E., Keltner, J. R., Weissleder, R., Rosen, B. R., and Weisskoff, R. M. (1998). Dynamic functional imaging of relative cerebral blood volume during rat forepaw stimulation. Magn. Reson. Med. *39*, 615–624.

S3. Vanduffel, W., Orban, G. A., Fize, D., Mandeville, J. B., Nelissen, K., Van Hecke, P., Rosen, B. R., and Tootell, R. B. (2001). Visual motion processing investigated using contrast agent-enhanced fMRI in awake behaving monkeys. Neuron *32*, 565–577.

S4. Rust, N. C., Mante, V., Simoncelli, E. P., and Movshon, J. A. (2006). How MT cells analyze the motion of visual patterns. Nat. Neurosci. *9*, 1421–1431.

S5. Willenbockel, V., Sadr, J., Fiset, D., Horne, G. O., Gosselin, F., and Tanaka, J. W. (2010). Controlling low-level image properties: The SHINE toolbox. Behav. Res. Methods *42*, 671–684.

S6. Dumoulin, S. O., and Wandell, B. A. (2008). Population receptive field estimates in human visual cortex. NeuroImage *39*, 647–660.

S7. Farivar, R., and Vanduffel, W. (2014). Functional MRI of awake behaving macaques using standard equipment. In Advanced Brain Neuroimaging Topics in Health and Disease - Methods and Applications, T. D. Papageorgiou, G. I. Christopoulos, and S. M. Smirnakis, eds.

S8. Fischl, B. (2012). FreeSurfer. NeuroImage *62*, 774–781.

S9. Mandeville, J. B., Choi, J.-K., Jarraya, B., Rosen, B. R., Jenkins, B. G., and Vanduffel, W. (2011). fMRI of cocaine self-administration in macaques reveals functional inhibition of basal ganglia. Neuropsychopharmacol. *36*, 1187–1198.

S10. Tsao, D. Y., Freiwald, W. A., Knutsen, T. A., Mandeville, J. B., and Tootell, R. B. H. (2003). Faces and objects in macaque cerebral cortex. Nat. Neurosci. *6*, 989–995.

S11. Benjamini, Y., and Hochberg, Y. (1995). Controlling the false discovery rate: a practical and powerful approach to multiple testing. J. Roy. Stat. Soc. B Met. *57*, 289–300.

S12. Polosecki, P., Moeller, S., Schweers, N., Romanski, L. M., Tsao, D. Y., and Freiwald, W. A. (2013). Faces in motion: selectivity of macaque and human face processing areas for dynamic stimuli. J. Neurosci. *33*, 11768–11773.

S13. Ernst, M. D. (2004). Permutation methods: a basis for exact inference. Stat. Sci. *19*, 676–685.

S14. Tsao, D. Y., Moeller, S., and Freiwald, W. A. (2008). Comparing face patch systems in macaques and humans. P. Natl. Acad. Sci. U.S.A. *105*, 19514–19519.

S15. Nelissen, K., Vanduffel, W., and Orban, G. A. (2006). Charting the lower superior temporal region, a new motion-sensitive region in monkey superior temporal sulcus. J. Neurosci. *26*, 5929–5947.

S16. Kolster, H., Mandeville, J. B., Arsenault, J. T., Ekstrom, L. B., Wald, L. L., and Vanduffel, W. (2009). Visual field map clusters in macaque extrastriate visual cortex. J. Neurosci. *29*, 7031–7039.

S17. Janssens, T., Keil, B., Farivar, R., McNab, J. A., Polimeni, J. R., Gerits, A., Arsenault, J. T., Wald, L. L., and Vanduffel, W. (2012). An implanted 8-channel array coil for high-resolution macaque MRI at 3T. NeuroImage *62*, 1529–1536.

S18. Handwerker, D. A., Gonzalez-Castillo, J., D'Esposito, M., and Bandettini, P. A. (2012). The continuing challenge of understanding and modeling hemodynamic variation in fMRI. NeuroImage *62*, 1017–1023.

S19. Jastorff, J., Popivanov, I. D., Vogels, R., Vanduffel, W., and Orban, G. A. (2012). Integration of shape and motion cues in biological motion processing in the monkey STS. NeuroImage *60*, 911–921.

S20. Leibovici, D. G., and Smith, S. (2000). Comparing groups of subjects in fMRI studies: a review of the GLM approach (Oxford, UK) Available at: http://www.fmrib.ox.ac.uk/analysis/techrep/tr00dl1/tr00dl1/index.html.

S21. Furl, N., Hadj-Bouziane, F., Liu, N., Averbeck, B. B., and Ungerleider, L. G. (2012). Dynamic and static facial expressions decoded from motion-sensitive areas in the macaque monkey. J. Neurosci. *32*, 15952–15962.

S22. Friston, K. J., Holmes, A. P., and Worsley, K. J. (1999). How many subjects constitute a study? NeuroImage *10*, 1–5.

S23. Holm, S. (1979). A simple sequentially rejective multiple test procedure. Scand. J. Stat. *6*, 65–70.